Spectral Energy Distributions of a Hard X-ray Selected AGN Sample in the Extended Groth Strip

Cristina Ramos Almeida[1], Jose Miguel Rodríguez Espinosa[1], Guillermo Barro[2], Jesús Gallego[2] y Pablo G. Pérez González[2]

[1] Instituto de Astrofísica de Canarias, [2] Universidad Complutense de Madrid

Abstract

We present ultraviolet to mid-infrared spectral energy distributions for a sample of 116 AGN selected both in X-rays and mid-infrared (96 with single detections and 20 with double optical counterparts) in the extended Groth strip. A complete set of different AGN types and starburst galaxy templates are used to fit the objects SEDs using the HyperZ photometric redshift code. Five main template groups are considered: Pure Starburst (24% of the sample), AGN contaminated by Starbursts (7 %), Type-1 AGN (21 %), Type-2 AGN (24 %), and Ellipticals & Spirals (24 %). Type-2 AGN and Ellipticals & Spirals sources are concentrated at low redshifts, whereas Pure Starburst and Type-1 AGN show a larger dispersion (objects have photometric redshifts ranging from z=0 to 3). This way, we have developed a reliable method of detection of starbursts at high redshifts coexisting with AGN. Correlations between hard/soft X-ray and ultraviolet, optical and infrared luminosities are reported, showing a noticeable improvement when only Type-1 AGN-fitted objects are considered. For the rest of the populations, these correlations get worse, probably due to the higher obscuration that affects the objects in these populations. For the 20 objects with double detections photometric redshifts have been also calculated. The percentage of Pure Starburst objects amongst this subset increases up to 48%.

Sample and multi-wavelength data.

The sample comprises 116 AGN taken from Barmby et al. (2006) in the extended Groth strip. These objects were selected in X-rays using data from Chandra and XMM-Newton, and all of them have secure detections in all four IRAC bands (Spitzer) in the mid-infrared, together with MIPS data in most of cases. Cross-matching of all sources between the X-ray, ultraviolet (GALEX), optical (CFHTLS), near-infrared (AEGIS), and mid-infrared have been performed. We find 96 sources with unique detections in all bands, plus another 20 objects with double detections in ground-based images.

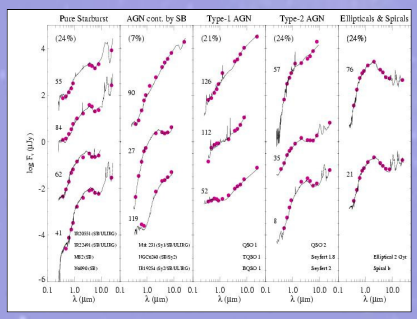


Fig. 1.- Examples of scaled SEDs in our sample (dots) fitted with different templates for the five groups considered. The X-axis corresponds to observed λ.

Spectral energy distributions and photometric redshifts of objects with unique detection.

We have classified the SEDs of the 96 objects with exclusive detections and estimated their photometric redshifts using the HyperZ photometric redshift code (Bolzonella, Miralles & Pelló 2000) to fit the library of starburst, AGN and galaxy templates from Polletta et al. (2007).

Examples of HyperZ fits for each one of the employed templates are shown in Fig. 1, divided in main five groups. The percentage found for each group is labelled.

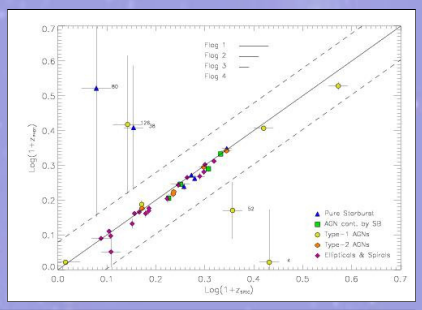


Fig. 2.- Comparison between photometric and spectroscopic redshifts for the 39 sources with z_{SPEC} from the DEEP data archive. The solid line corresponds to z_{SPEC} $=z_{SPEC}$. Horizontal error bars indicate the reliability of the z_{SPEC} (flag = 1 for the less reliable). The five outliers are labelled (note that there are not outliers when only the 28 galaxies with reliable z_{SPEC} are considered).

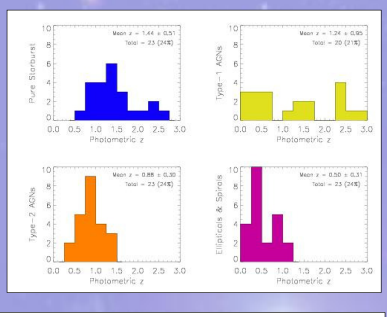


Fig. 3.- Histograms for the Pure Starburst, Type-1 AGN, Type-2 AGN, and Elliptical & Spirals groups. Mean photometric redshift, together with the number of objects included in each group are reported in each panel.

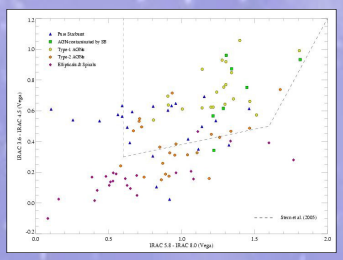
Band	Total fit Hard X-ray	Pure SB Hard X-ray	AGN cont. SB Hard X-ray	Type-1 AGN Hard X-ray	Type-2 AGN Hard X-ray	Ell/S Hard X-ray
	α r	α r	α r	α r	α r	α r
FUV	1.228 0.842	1.055 0.811	1.308 0.911	1.289 0.947	- -	1.092 0.715
NUV	0.836 0.726	1.083 0.827	0.886 0.872	0.993 0.848	- -	0.766 0.658
u	0.754 0.726	0.899 0.788	- -	1.009 0.892	- -	- -
g	0.705 0.725	0.788 0.716	1.117 0.799	0.989 0.910	0.759 0.584	- -
r	0.668 0.713	0.710 0.657	- -	0.974 0.919	0.712 0.569	- -
i	0.646 0.726	0.709 0.645	- -	0.964 0.926	0.636 0.551	0.491 0.607
z	0.673 0.733	0.783 0.737	- -	0.967 0.929	0.640 0.590	0.501 0.603
J	0.688 0.748	0.818 0.790	- -	0.966 0.937	0.703 0.622	0.513 0.616
K	0.718 0.784	0.785 0.820	1.250 0.875	0.983 0.917	0.661 0.530	0.645 0.697
IRAC3.6	0.814 0.799	1.007 0.834	1.396 0.878	0.991 0.957	0.667 0.494	0.776 0.692
IRAC4.5	0.866 0.796	1.072 0.917	- -	0.896 0.856	0.770 0.510	0.859 0.699
IRAC5.8	0.907 0.786	0.963 0.735	1.382 0.842	0.905 0.913	0.811 0.526	0.892 0.672
IRAC8.0	0.931 0.794	0.694 0.645	1.399 0.851	0.919 0.875	0.824 0.556	0.984 0.702
MIPS24	1.014 0.695	- -	- -	0.886 0.836	0.874 0.901	1.224 0.673

Band	Total fit Soft X-ray	Pure SB Soft X-ray	AGN cont. SB Soft X-ray	Type-1 AGN Soft X-ray	Type-2 AGN Soft X-ray	Ell/S Soft X-ray
	α r	α r	α r	α r	α r	α r
FUV	1.073 0.834	0.925 0.893	0.919 0.948	1.175 0.951	- -	0.903 0.641
NUV	0.753 0.738	0.970 0.854	- -	0.972 0.956	- -	0.722 0.568
u	0.669 0.729	0.703 0.760	- -	0.974 0.890	- -	- -
g	0.618 0.710	0.638 0.720	- -	0.954 0.900	- -	- -
r	0.593 0.698	- -	- -	0.936 0.903	- -	- -
i	0.574 0.700	- -	- -	0.926 0.908	- -	0.456 0.602
z	0.576 0.703	- -	- -	0.929 0.911	- -	0.471 0.609
J	0.590 0.717	0.518 0.651	- -	0.923 0.915	- -	0.471 0.610
K	0.621 0.763	0.489 0.671	- -	0.791 0.919	- -	0.574 0.673
IRAC3.6	0.705 0.783	0.639 0.706	- -	0.794 0.985	- -	0.687 0.670
IRAC4.5	0.757 0.786	0.726 0.738	- -	0.799 0.971	- -	0.752 0.669
IRAC5.8	0.793 0.774	0.725 0.721	- -	0.807 0.968	- -	0.779 0.640
IRAC8.0	0.796 0.770	0.579 0.674	- -	0.810 0.982	- -	0.825 0.641
MIPS24	0.885 0.678	0.663 0.614	- -	0.766 0.941	- -	1.033 0.626

Table 2: Photometric band, fit slope and correlation coefficient r of the scatter diagrams between the FUV, NUV, ugriz, J, K, IRAC and MIPS bands and the hard and soft X-ray luminosities for the total fit, *Pure Starburst*, *AGN contaminated by Starbursts*, *Type-1 AGN*, *Type-2 AGN* , and *Ellipticals & Spirals* groups. GALEX bands are not include[1] because correlations are not significant. Spearman's rank correlation tests have been performed for all scatter diagrams. The values reported in Table 2 are indeed significant ($p<0.01$).

Correlations.

If the active nucleus is the dominant source at all wavelengths, tight linear correlations should be drawn. However, AGN are hosted by different galaxies, that contaminate and mask them, deviating the correlations from linear and worsening them. Both the X-ray and the mid-infrared emissions are mostly dominated by the active nucleus, whereas the optical and the near-infrared are more affected by extinction or by stellar emission. This is clearly reflected in the first row of Table 1. We also reported slopes and correlation coefficients for the five main groups considered. Type-1 AGN-fitted objects display the most tight and linear correlations of the sample, what gives confidence in our fits.



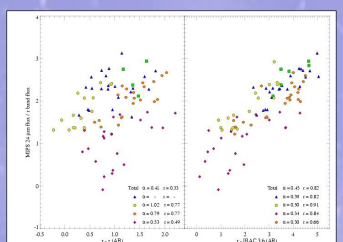


Fig. 4.- IRAC color-color plot for the 96 sources in the sample. The dashed line corresponds to Stern et al. (2005) empirical segregation of AGN. Type-1 AGN are all contained in this region. There are many SB and Type-2 AGN inside also, with higher mean redshifts than those in the same groups that are outside the dashed lines.

Fig. 5.- Mid-infrared to optical ratio versus the r-z and r-IRAC 3.6 colors. The most obscured objects (Pure SB and Type-2 AGN) are located at the upper-right corner of both figures.

References.

Barmby, P., et al. 2006, ApJ, 642, 126

Bolzonella, M., Miralles, J.-M., & Pelló, R. 2000, A&A, 363, 476

Polletta, M. et al. 2007, ApJ, 663, 81

Stern, D., et al. 2002, ApJ, 568, 71